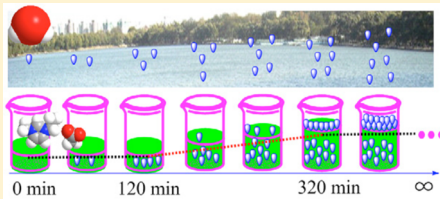


The Dynamic Process of Atmospheric Water Sorption in [BMIM][Ac]: Quantifying Bulk versus Surface Sorption and Utilizing Atmospheric Water as a Structure Probe

Yu Chen, Yuanyuan Cao, Chuanyu Yan, Yuwei Zhang, and Tiancheng Mu*

Department of Chemistry, Renmin University of China, Beijing 100872, P. R. China

ABSTRACT: The dynamic process of the atmospheric water absorbed in acetate-based ionic liquid 1-butyl-3-methyl-imidazolium acetate ([BMIM][Ac]) within 360 min could be described with three steps by using two-dimensional correlation infrared (IR) spectroscopy technique. In Step 1 (0–120 min), only bulk sorption via hydrogen bonding interaction occurs. In Step 2 (120–320 min), bulk and surface sorption takes place simultaneously via both hydrogen bonding interaction and *van der Waals* force. In Step 3, from 320 min to steady state, only surface sorption via *van der Waals* force occurs. Specifically, Step 2 could be divided into three substeps. Most bulk sorption with little surface sorption takes place in Step 2a (120–180 min), comparative bulk and surface sorption happens in Step 2b (180–260 min), and most surface sorption while little bulk sorption occurs in Step 2c (260–320 min). Interestingly, atmospheric water is found for the first time to be used as a probe to detect the chemical structure of [BMIM][Ac]. Results show that one anion is surrounded by three C₄H molecules and two anions are surrounded by five C₂H molecules via hydrogen bonds, which are very susceptible to moisture water especially for the former one. The remaining five anions form a multimer (equilibrating with one dimer and one trimer) via a strong hydrogen bonding interaction, which is not easily affected by the introduction of atmospheric water. The alkyl of the [BMIM][Ac] cation aggregates to some extent by *van der Waals* force, which is moderately susceptible to the water attack. Furthermore, the proportion of bulk sorption vs surface sorption is quantified as about 70% and 30% within 320 min, 63% and 37% within 360 min, and 11% and 89% until steady-state, respectively.



1. INTRODUCTION

Ionic liquids (ILs) have drawn increasing attention because of their high greenness and tunability compared to volatile organic compounds (VOCs).¹ Acetate-based ILs (AcILs) show a higher ability for biomass (e.g., cellulose^{2–4} and chitosan^{5–7}) dissolution than other types of ILs or common solvents. During this process, the role of water cannot be ignored. Water could be used as an antisolvent to regenerate biomass from AcILs, and mixing water with AcIL would prohibit the dissolution of biomass.^{7–13} Also, the physical property and chemical structure of AcILs would be altered dramatically in the presence of water.^{14–16}

Therefore, water contamination should be avoided for the biomass dissolution in AcILs. However, most ILs are able to absorb some extent of water from moist air.^{17–23} Especially, AcILs show a higher hygroscopicity than other ILs.^{20,24} For example, 1-butyl-3-methyl-imidazolium cholate [BMIM]-[CHO] absorbed only 0.72% g H₂O/g ILs, while the AcIL 1-butyl-3-methyl-imidazolium acetate [BMIM][Ac] could absorb as much as 15.63% g H₂O/g ILs.²⁰ Thus, conclusion could be drawn that it would be unavoidable for such hygroscopic AcILs to make contact with the ubiquitous atmospheric water in the process of synthesis, storage, or transportation.

The interaction between atmospheric water and AcILs would affect the application of biomass processed by AcILs. Several researches have been carried out on the interaction mechanisms between AcILs and water. For example, Craig²⁵ found that the

mixing process of water and AcILs was exothermic with no new compounds formed, but there was a possibility that one AcIL was surrounded by three water molecules. Ding²⁶ concluded that AcILs mainly interacted with water by hydrogen bonds between the anion of ILs and water. Brehm²⁷ found that the hydrogen bond net work, carbenes, and dipole moment of AcILs were modified and disturbed after the addition of water.

These researches were all conducted by adding water into the AcILs manually;^{25–30} however, the *in situ* process of atmospheric water absorbed in AcILs has not been studied. The atmospheric water sorption process in AcILs is more practical and more common, which is important for the utilization and regeneration of biomass. Thus, in this study, the moisture water sorption mechanism by AcILs is investigated by choosing [BMIM][Ac] (Scheme 1) as a typical AcIL.

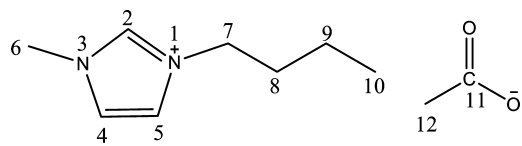
Furthermore, various analytic technologies have been applied to explore interactions between ILs and solvents, such as infrared spectroscopy (conventional FTIR, difference IR (Diff-IR), excessive IR, and two-dimensional correlation (2D-COS) IR);^{18,22,31–43} nuclear magnetic resonance (NMR) and 2D-NMR;^{25,43–45} density functional theory (DFT) and Monte Carlo simulation;^{27,28,32,37,42} X-ray scattering and neutron scattering,^{45,46} conventional and excessive thermodynamic

Received: March 26, 2014

Revised: April 25, 2014

Published: May 19, 2014

Scheme 1. Chemical Structure and Notation of 1-Butyl-3-methyl-imidazolium Acetate [BMIM][Ac]



property measurement.^{47–50} Among all these analytical methods, IR is very sensitive to the hydrogen bonds. Generalized 2D-COS (G-2D-COS, by Noda) could be employed for detecting a dynamic interaction process only by

comparing the average rate of change of two spectra variables, which is plotted as a plane consisting of two spectra variables.^{51,52} Autocorrelation moving-window 2D-COS (auto-MW2D-COS, by Thomas⁵³) and perturbation-correlation moving-window 2D-COS (PCM2D-COS, by Morita⁵⁴) techniques were further developed to justify the critical point after introducing the perturbation variable axis. Water sorption by [BMIM][Ac] from atmospheric moisture is a dynamic process related to hydrogen-bonding interactions that might also contain critical points. Thus, the conventional FTIR, Diff-IR, G-2D-COS IR, auto-MW2D-COS IR, and PCM2D-COS IR spectroscopies were applied to explore the dynamic process

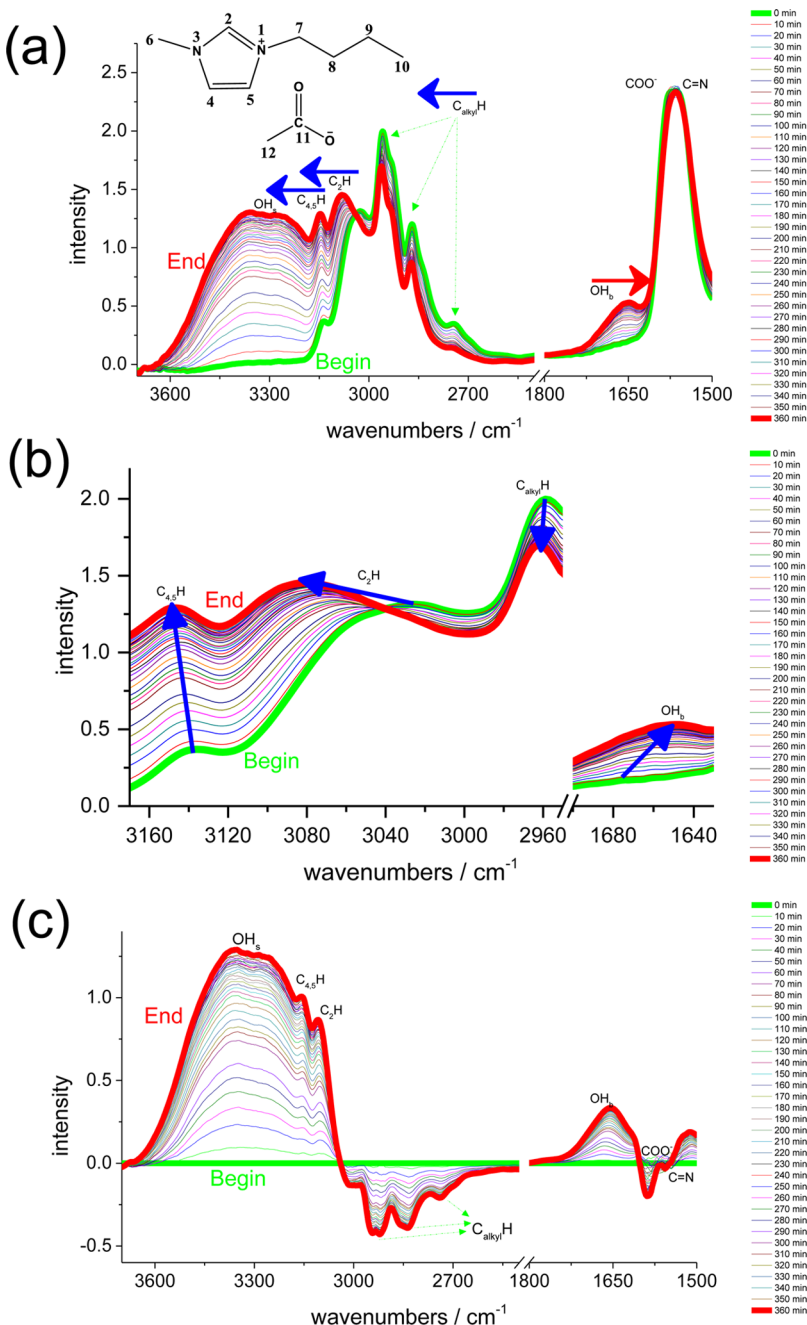


Figure 1. Normal (a), partially enlarged normal (b), and difference (c) infrared IR spectroscopy of pure ILs [BMIM][Ac] before and after absorbing atmospheric water as a function of time within 360 min. The difference spectroscopy is referred to the pure ILs [BMIM][Ac]. The arrow in red and blue color indicate red and blue shift of absorption peak, respectively.

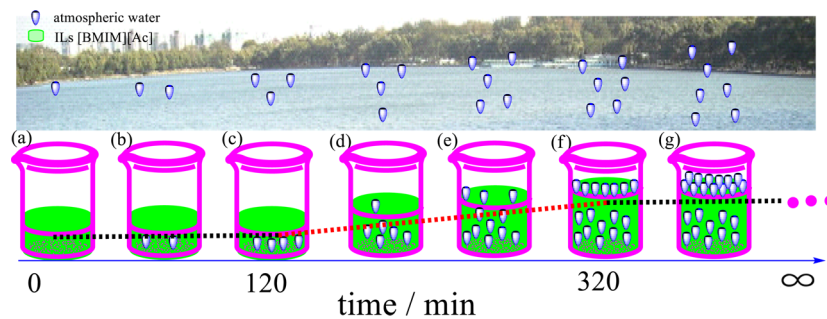


Figure 2. Proposed dynamical atmospheric water sorption mechanism in [BMIM][Ac].

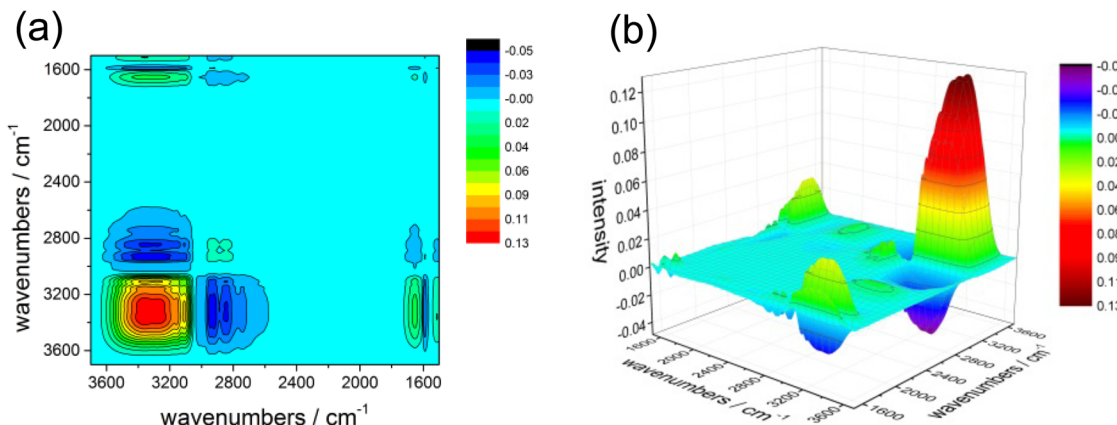


Figure 3. Planar (a) and stereoscopic (b) synchronous generalized two-dimensional correlation spectroscopy (s-G-2D-COS).

and critical points of the [EMIM][Ac]–atmospheric water interaction.

The work is described as follows. First, the dynamic process of the absorption of atmospheric water by [BMIM][Ac] is analyzed. Then, by using atmospheric water as a probe, the chemical structure of [BMIM][Ac] in its pure state is deduced. Following, we give a microscopic explanation for the dynamic water sorption process, mainly from the perspective of bulk sorption versus surface sorption, hydrogen bonding interaction versus van der Walls force. Finally, quantification of bulk and surface atmospheric water sorption in [BMIM][Ac] at a specific time point (i.e., 320 min, 360 min, and steady-state) is derived.

2. EXPERIMENTAL SECTION

2.1. Materials. [BMIM][Ac] (purity > 99%) was supplied by Lanzhou Greenchem ILs, LICP, CAS (Lanzhou, China). It was put in a vacuum oven at 65 °C for 90 h before use, with some extent of P₂O₅ nearby. The impurities were measured after drying and were described as follows. Water content was less than 620 ppm measured by Karl Fisher titration. Halogen ion was undetectable by AgNO₃ precipitation. Other impurities were also undetectable by NMR, Bruker AM 400 MHz spectrometer. The NMR spectra and IR spectra before and after drying were also conducted. The unchangeable result indicated that thermal decomposition of the [BMIM][Ac] during the drying process was negligible.

2.2. ATR-IR Spectra. The attenuated total reflection infrared (ATR-IR) spectra (Prestige-21 FTIR spectrometer, Shimadzu, Japan) of [BMIM][Ac] exposed to the moisture air were measured immediately after [BMIM][Ac] without stirring was placed on the instrument. Then, this sample was scanned every 10 min up to 360 min, after which the change of intensity

and positions of all peaks was negligible. Each sample was analyzed for 40 scans. The ATR-IR detector was a DTGS with a resolution 4 cm⁻¹. The wavenumber range was from 4600 to 400 cm⁻¹. The incident angles of the ATR cell (ATR-8200H, made of ZnSe) were 45°. [BMIM][Ac] covered 584 mm² surfaces on top of the crystal. The experimental process was conducted at room temperature (*T*, about 25 °C) and 35% (relative humidity, RH) on average, detected by a temperature and humidity sensor (Testo 608-H2, Germany with the precision of ±0.2 °C, ±2% RH)

2.3. G-2D-COS, Auto-MW2D-COS, and PCMW2D-COS. G-2D-COS, auto-MW2D-COS, and PCMW2D-COS were calculated using 2D shige software (<http://sci-tech.ksc.kwansei.ac.jp/~ozaki/2D-shige.htm>). The window size (2*m* + 1) for the 2D-COS calculation was set as 11.

3. RESULTS AND DISCUSSION

The summaries of figures were first described as below. Figure 1 gives the conventional and difference IR spectra of [BMIM][Ac]. The three-step dynamic water sorption process is described in Figure 2. The synchronous G-2D-COS (s-G-2D-COS), asynchronous G-2D-COS (as-G-2D-COS), auto-2D-COS, synchronous PCMW2D-COS (s-PCMW2D-COS), and asynchronous PCMW2D-COS (as-PCMW2D-COS), are given in Figures 3–7, respectively. The quantification of bulk vs surface water sorption is shown in Figure 8. The interpretation of 2D-COS is according to Noda's Rule^{51,52} (for G-2D-COS) and Morita's Rule⁵⁴ (for auto-MW2D-COS and PCMW2D-COS).

3.1. Interpreting 1D-IR and 2D-COS IR of [BMIM][Ac]–Atmospheric Water. The IR assignments of the [BMIM][Ac]–atmospheric water system are referred to other previous

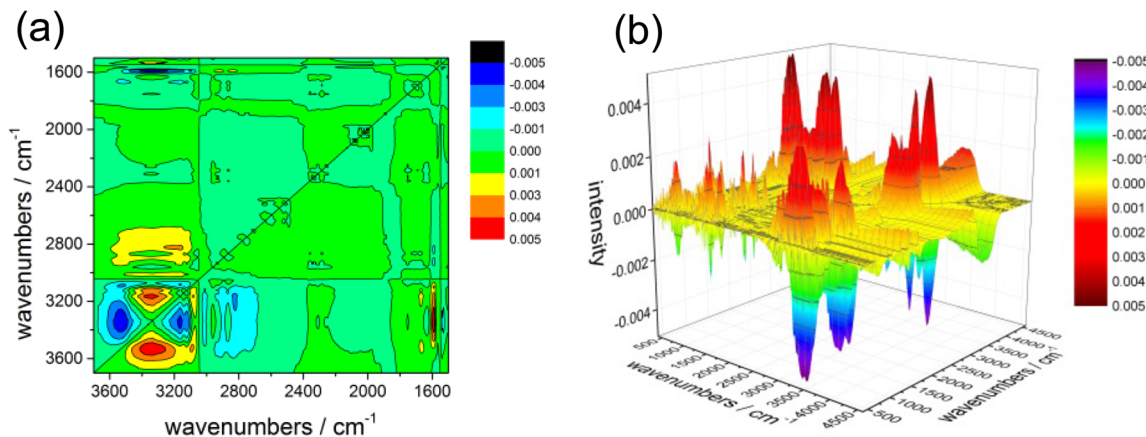


Figure 4. Planar (a) and stereoscopic (b) asynchronous generalized two-dimensional correlation spectroscopy (as-G-2D-COS).

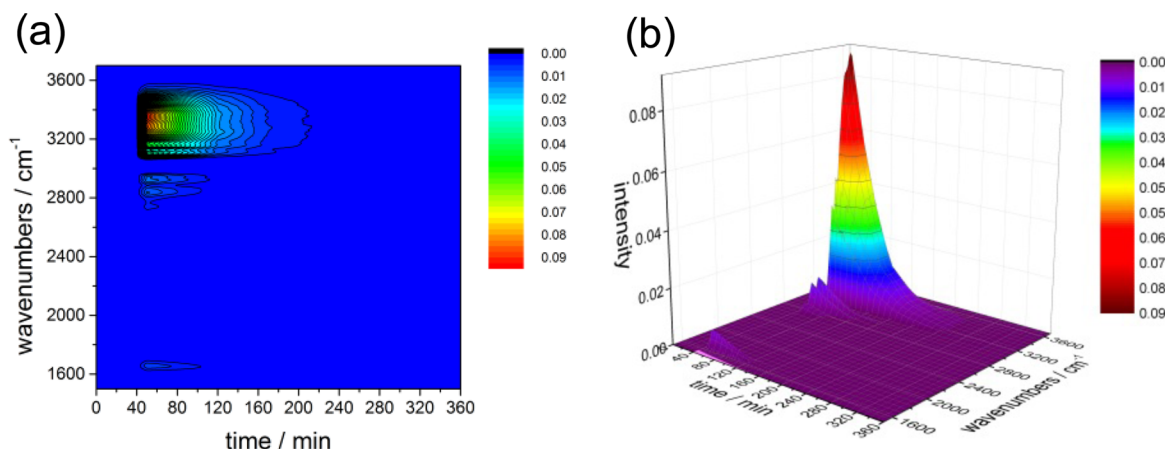


Figure 5. Planar (a) and stereoscopic (b) autocorrelation moving-window two-dimensional correlation spectroscopy (auto-MW2D-COS).

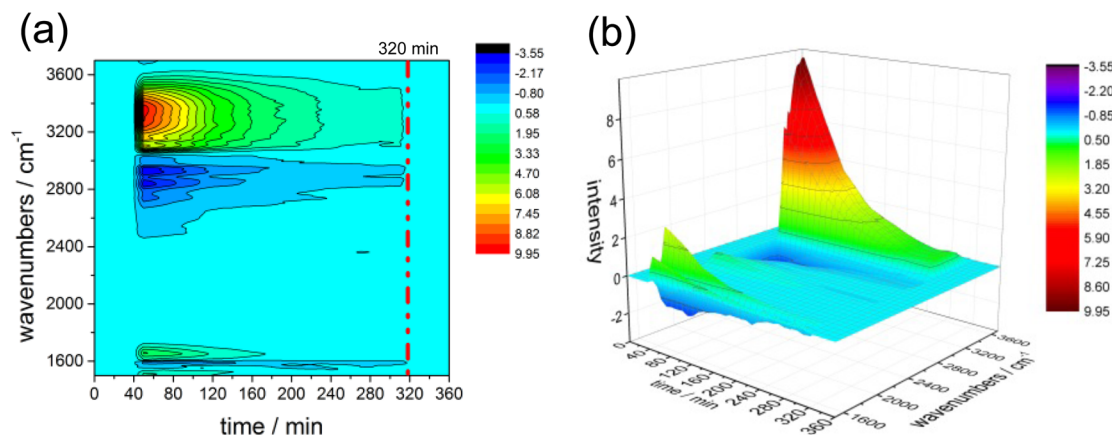


Figure 6. Planar (a) and stereoscopic (b) synchronous perturbation-correlation moving-window two-dimensional correlation spectroscopy (s-PCM2D-COS).

reports of some similar ILs (e.g., [EMIM][Ac] with the same anion and [BMIM][BF₄] with the same cation, compared to [BMIM][Ac]): OH stretching vibration (OH_s) of water absorbed in [BMIM][Ac] at ca. 3300 cm⁻¹ (specifically, the peak position of the asymmetric mode is higher than that of symmetric mode),^{22,26} OH bending vibration (OH_b) water absorbed in [BMIM][Ac] at ca. 1645 cm⁻¹,²⁶ COO⁻ asymmetric stretching vibration at ca. 1560 cm⁻¹,²⁶ over 3000 cm⁻¹ for cation ring H (i.e., C2H, C4SH) stretching vibration

and less than 3000 cm⁻¹ for alkyl H (i.e., C6, 7, 8, 9, 10H) peak position.³⁶ Specifically, C2H of the cation ring has a stronger hydrogen-bonding interaction with the anion than C4SH, thus the IR vibration frequency of C2H should be lower than that of C4SH. This is consistent with our IR experimental observations (Figure 1). Furthermore, the alkyl H (C6,7,8,9,10H) has a lower electron density, hence a weaker force constant, than the imidazolium cation ring H (i.e., C2,4,5H). The corresponding IR peak absorption of the alkyl H

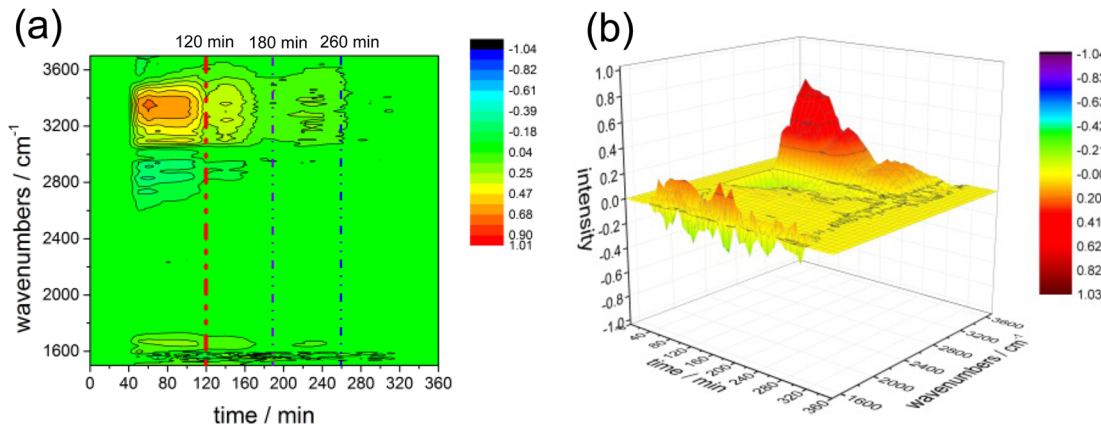


Figure 7. Planar (a) and stereoscopic (b) asynchronous perturbation-correlation moving-window two-dimensional correlation spectroscopy (as-PCMW2D-COS).

should also be vibrated at a lower frequency, which is also the same with our experimental results (Figure 1). The peak position of OH_s is ca. 3300 cm⁻¹, much resembling that of pure water with a water network.^{22,55} It indicates that apart from hydrogen-bonding to the acetate anion of [BMIM][Ac], water might also form a hydrogen-bonding network with water already dissolved in [BMIM][Ac], but the critical point to discriminate among water-anion and water-water hydrogen bonds will be discussed later.

The changes in peak position shown in Figure 1 are listed as red shift (OH_b), blue shift (C2H, C4,5H and C_{alkyl}H), and negligible shift (OH_s, COO⁻, and C=N). Specifically, C2H shows the most extent of peak shifts (Figure 1b). The change in peak intensity is listed as decrease (C_{alkyl}H), increase (OH_s, OH_b, C2H and C4,5H), and negligible alternation (COO⁻ and C=N). An average sequence for the IR peak could be obtained by combining s-G-2D-COS (Figure 3) and as-G-2D-COS (Figure 4) within 360 min. The peak intensity change rate without considering the change direction along with the time perturbation variable gained via auto-MW2D-COS (Figure 5) is ordered as OH_s > C4,5H > C2H > C_{alkyl}H > OH_b > COO⁻, C=N. Considering the change direction of intensity along with time perturbation variable, s-PCMW2D-COS (Figure 6) gave a detail as positive correlation (OH_s, C4,5H, C2H and OH_b), negative correlation (C_{alkyl}H), and almost no correlation (COO⁻ and C=N). The turning points could be determined by the as-PCMW2D-COS in Figure 7.

3.2. Dynamical Process of Atmospheric Water Sorption. Before we point out the bulk and surface atmospheric water sorption in [BMIM][Ac] (possibly for other ILs) by these assumptions discussed later, it is admitted that water molecules directly interact with ILs by hydrogen bonds and water molecules involved in a liquid water network, then interact with other water molecules.

Figure 6 shows that before 320 min the value of s-PCMW2D-COS changed significantly, while after that the value remains almost constant, which indicates that 320 min is a turning point. The possible reason is that the atmospheric water is mainly absorbed into the bulk of [BMIM][Ac] before 320 min, while it stays on the surface of [BMIM][Ac] after that until steady state. It should be noted that the intensity of OH_b around 1650 cm⁻¹ shows an earlier turning point at 180 min (rather than 320 min) in Figure 6. A more detailed explanation about this earlier turning point would be discussed later.

Another turning point is found in the as-PCMW2D-COS of the [BMIM][Ac]/water IR spectra at 120 min (Figure 7). Before 120 min, all the peaks along the time perturbation variable increase with increasing rate of intensity; but less increasing rate occurs after 120 min. The increase of water capacity before 120 min could be entirely ascribed to bulk sorption, while simultaneous bulk and surface water sorption would occur after 120 min.

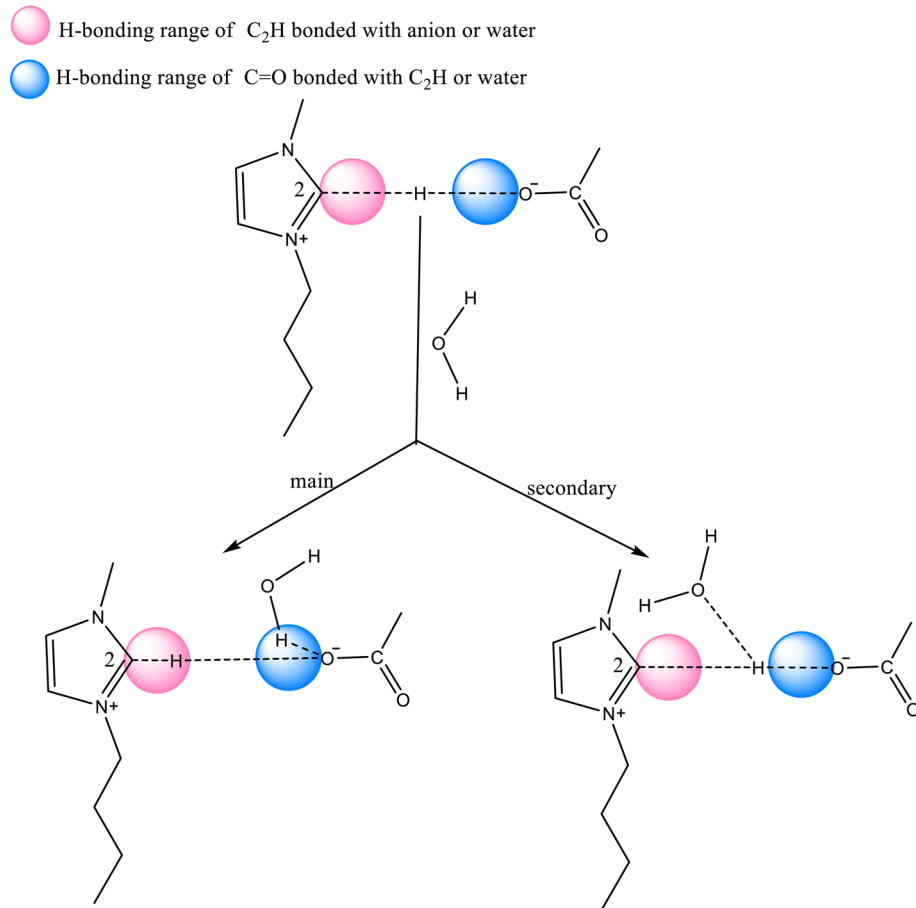
Thus, the dynamic process of water sorption could be divided into three steps (Figure 2). The first 120 min is Step 1, where only bulk water sorption occurs. From 120 to 320 min, bulk and surface sorption happen simultaneously (Step 2). In Step 3, only surface sorption takes place (320 min to steady state).

Interestingly, the existence of two minor turning points at 180 and 260 min (Figure 7) shows that Step 2 could be divided into three substeps, that is, Step 2a (120–180 min), Step 2b (180–260 min), and Step 2c (260–320 min). Particularly, Figure 6 also shows that 180 min is the turning point for an anion possessing undetectable change in intensity, which gives more evidence for the substeps. Step 2a, 2b, and 2c correspond to most bulk sorption, comparative bulk and surface sorption, and most surface sorption, respectively.

Note that we do not by any means claim that we have experimentally proven the existence of a three-step atmospheric water sorption process in [BMIM][Ac] via 2D-COS (including G-2D-COS, auto-MW2D-COS, and PCMW2D-COS) IR spectroscopy. The truth is that we try to interpret their experimental observations in terms of some dual (surface/bulk) sorption mechanism; more work is needed to make this proposed three-step mechanism clearer.

3.3. Atmospheric Water Is a Probe for Chemical Structure of [BMIM][Ac]. A probe is a substance put in an environment to detect a change in environment. Both the IR peak intensity and peak position of ILs are changed in the presence of atmospheric water. That is, atmospheric water could be deemed as a probe for the chemical structure of ILs via IR spectra. Note that if much atmospheric water is absorbed, the structure change in ILs could not reflect the pure ILs but the water-absorbed ILs. In this sense, Step 1 is used to analyze the chemical structure of [BMIM][Ac]. Additionally, Step 1 from 0 to 120 min has the advantage of entire bulk sorption, refraining from the intervention by external and indirect factors, that is, surface sorption.

Scheme 2. Effect of Water on the Hydrogen-Bonding Interaction between C_{2,4,5H} of the BMIM Cation and C=O of the Acetate Anion Illustrated by C_{2H}

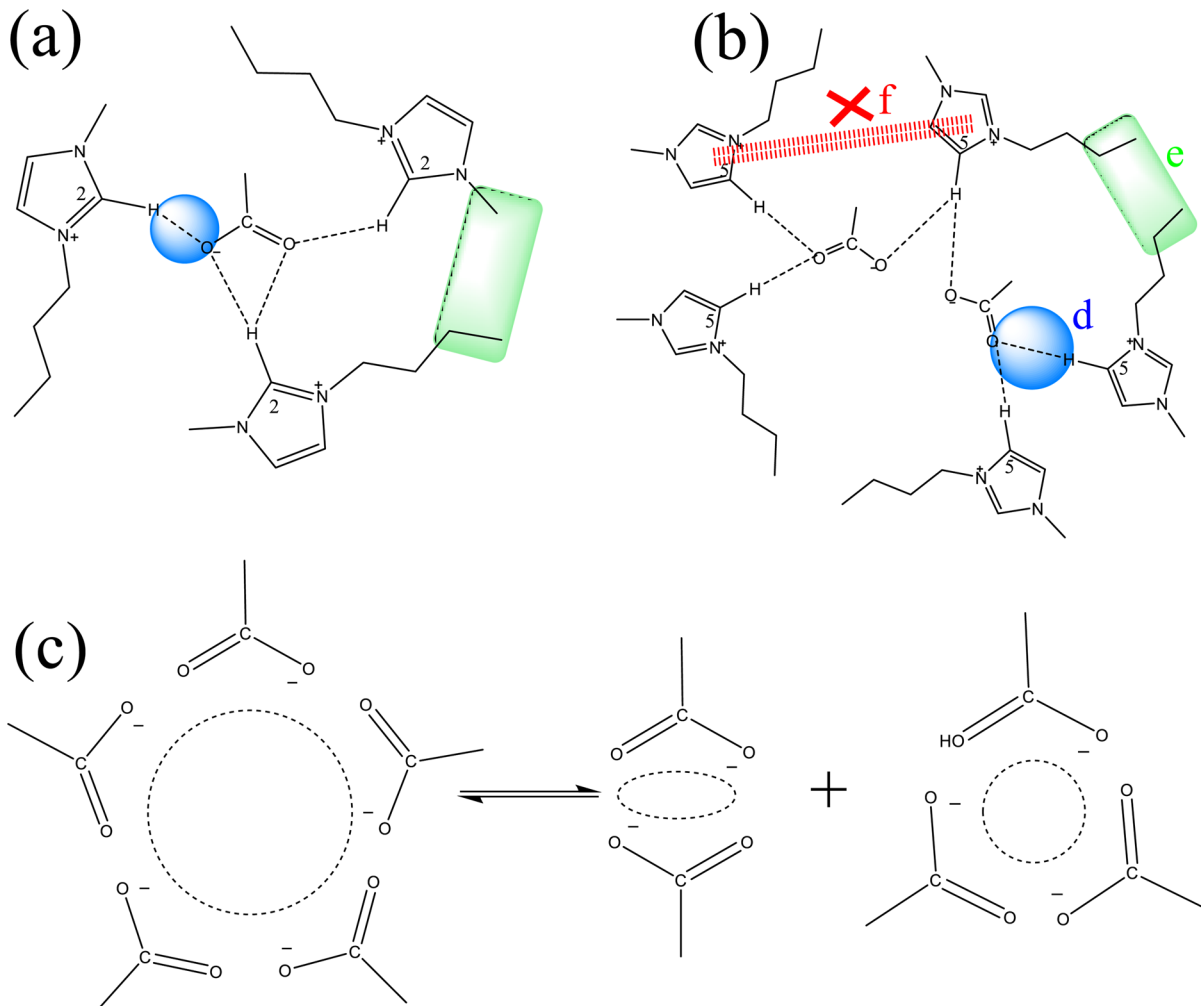


A new band OH_b around 1650 cm⁻¹ is formed with a red shift and increasing peak intensity as a function of time in Step 1 (Figure 1). It could be totally ascribed to the hydrogen bonding interaction between water and anion COO⁻ in this step. In this way, OH_b could be used to approximately indicate the changeable part in the chemical environment of anion COO⁻, which is helpful to deduce the chemical structure of [BMIM][Ac] discussed later. The blue shift and increasing peak intensity of C_{2,4,5H} (Figure 1) indicate that C_{2,4,5H} is anion-free after the anion is hydrogen-bonded with water (Scheme 2). It implies an increase in the amount of and the strength of C_{2,4,5H}. Positive (C_{2,4,5H}, OH_b) of s-G-2D-COS (Figure 3) and as-G-2D-COS (Figure 4) means an average prior change for C_{2,4,5H} than for OH_b by Noda's Rule. A higher average increasing rate of peak intensity for C_{2,4,5H} than for OH_b could also be corroborated semiempirically by the change of the corresponding difference spectra in Figure 1. It could thus be deduced that there are several C_{2,4,5H} around one anion in pure [BMIM][Ac]; several cations would be released once the atmospheric water attacks one anion.

Specifically, intensity-increasing rate of C_{4,5H} (ca. 2.77 times that of OH_b) is higher than that of C_{2H} (ca. 2.44 times that of OH_b) (Figures 1 and 6). It means that there are more newly C_{4,5H} formed than C_{2H} upon the perturbation of atmospheric water, that is, about three C_{4,5H} molecules surrounded by one anion (Scheme 3a), and five C_{2H} molecules surrounded by two anions (Scheme 3b). The former conclusion is consistent with that drawn by Bowron⁵⁶ illustrated with a shorter chain

[EMIM][Ac], where one anion probably associates with three H of the imidazolium ring. The blue-shifting rate of C_{4,5H} is lower than that of C_{2H} (see enlarged Figure 1b), which means that the interaction of the C_{4,5H}/anion is weaker than that of the C_{2H}/anion. The above discussions suggest that one anion is surrounded by several C_{4,5H} with weak interactions, or surrounded by less C_{2H} with strong interactions. The remaining five anions (equaling to the difference between eight cations and three anions) would form a stable multimer (i.e., pentamer, equilibrating with one dimer and one trimer) by strong hydrogen-bonding interaction (Scheme 3c), free from the perturbation of atmospheric water. This can be corroborated in Figure 1 by the unchanged COO⁻ around 1560 cm⁻¹ and by the lower peak position of COO⁻ (1560 cm⁻¹, among five anions) than the newly formed OH_b (1650 cm⁻¹, water with one anion).

However, C_{alkyl}H in the cation shows a different tendency compared to that of cation ring H (i.e., C_{2H}, C_{4,5H}). Figure 1 shows that C_{alkyl}H decreases its intensity (opposite to cation ring H) but shifts to a higher wavenumber (the same with cation ring H). It means that the interactions of C_{alkyl}H/anion and C_{2,4,5H}/anion are different after introducing the atmospheric water. In this case, it is not favorable for C_{alkyl}H to form hydrogen bonds with an anion, whereas C_{alkyl}H could form a nonpolar domain by a weak van der Waal force (Scheme 4), which could be reduced by the expansion of the nonpolar domain after absorbing water (Scheme 4). Thus, the decreasing intensity of C_{alkyl}H could be explained by the concentration

Scheme 3. Derived Most Probable Chemical Structure of Pure IL [BMIM][Ac]^a

^aDetected by using atmospheric water as the probe via IR spectra: one acetate anion surrounded by two C₂H (a), two acetate anion surrounded by five C₄H or C₅H (b), pentamer composed by five acetate anions, equilibrating with one dimer and one trimer (c), hydrogen-bonding interaction between acidic hydrogen and anion (d, illustrated with two blue circles), van der Waals force among alkyl chain of cation (e, illustrated with two green rectangles), unfavorable ring–ring stack among cation rings (f, illustrated with one red double-dotted line).

lowering effect after water absorption and no new formation of $\text{C}_{\text{alkyl}}\text{H}$ (while $\text{C}_{2,4,5}\text{H}$ has a dominating newly formed effect over concentration lowering effect. The blue shift of $\text{C}_{\text{alkyl}}\text{H}$ is the result of reduced van der Waals force among them (while $\text{C}_{2,4,5}\text{H}$'s blue shift is due to their freedom after water robbing their originally bounded anion).

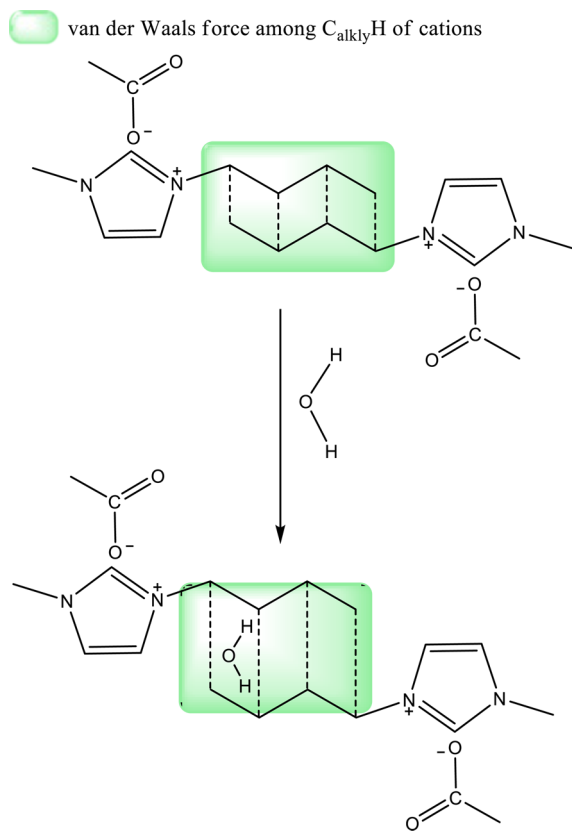
The cation–cation stacking in pure [BMIM][Ac] could also be derived. IR absorption peak $\text{C}=\text{N}$ (around 1560 cm^{-1} , coupled with COO^-) reflects the chemical environment of the imidazolium cation ring. Figure 1 shows that the change in peak position and peak intensity of $\text{C}=\text{N}$ is negligible after absorbing trace of water. It is possible due to the negligible ring–ring piling. It is reasonable because the anion/ $\text{C}_{2,4,5}\text{H}$ interaction and nonpolar domains among several $\text{C}_{\text{alkyl}}\text{H}$ (as shown in Scheme 3) are not favorable for the formation of a ring–ring stack. Also, the cation ring is positively charged, so, they would repel with each other to some extent, which disfavors the stacking of ring–ring.

3.4. Microscopic Explanation for the Dynamic Atmospheric Water Sorption Process. Step 1 is referred to a total bulk water sorption in [BMIM][Ac], as shown in Figure 2. The entire bulk sorption at the first 120 min (Step 1)

indicates that interaction between water and [BMIM][Ac] is the strongest in the corresponding time region. This interaction is possibly the water–anion hydrogen-bonding interaction because of their stronger interaction than water–C₂H, water–C_{4,5}H, and water– $\text{C}_{\text{alkyl}}\text{H}$, as discussed before. After this step (i.e., after 120 min), water might also interact with other water molecules and form a stronger hydrogen-bonding network, hence a red shift of peak position in Figure 1. Specifically, this hydrogen-bonding network of water is not negligible until 180 min, as shown by the turning point in Figure 6. The strong interaction might induce negligible volume increase due to the load of water in the free space of [BMIM][Ac]. Therefore, peak intensity and peak position are altered for OH, C₂H, C_{4,5}H, and $\text{C}_{\text{alkyl}}\text{H}$ (Figures 1, 5, and 6). Owing to the higher strength of hydrogen bonds, a robust water sorption could be seen for many ILs to absorb moisture water initially. Our previous hygroscopicity experiments also suggested that the initial water sorption rate (nearly linearly) is faster than that of the time period afterward.²⁰ On the other hand, removing this part of water would be very difficult.

Step 3 (320 min to steady state) is the process of surface water sorption in [BMIM][Ac] as shown in Figures 2f,g. The

Scheme 4. Effect of Water on the van der Waals Interaction among C_{alkyl}H (i.e., C_{6,7,8,9,10H}) of the BMIM Cations Illustrated by C_{7, 8, 9, 10H}



turning point at 320 min could be corroborated in the s-PCM2D-COS (Figure 6), while this turning point to divide bulk sorption and surface sorption is hard to determine by only eye visualization, probably due to the higher accuracy of s-PCM2D-COS than simple eye visualization. In this process, atmospheric water only interacts with the surface of [BMIM]-[Ac] by van der Waals force, which is weaker than the hydrogen bonds in Step 1, and therefore the bulk [BMIM][Ac] is not affected by the moisture. Similarly, the volume of the bulk phase would not be altered because of the surface water sorption. The possible reason might be due to the reach of the volume expansion limit after 320 min. The absorbed bulk water prohibit [BMIM][Ac] to absorb more water into the bulk part. Other reasons could be the relative high viscosity and surface tension of [BMIM][Ac]. Also note that there is no mechanic mixing or stirring device in the whole process, deterring again the atmospheric water from percolating inside the [BMIM]-[Ac] sample. It might also be caused by the generation of a film on the [BMIM][Ac] by atmospheric water,¹⁹ and this generated film would reduce the atmospheric water to enter into the bulk [BMIM][Ac] further. The IR spectra of the peak intensities and positions thus remain almost unchanged (Figures 1, 5, and 6); all the bands varying in this step could thus be due to the liquid absorbed atmospheric water (including OH stretching (OH_s), and OH bending (OH_b) vibration) other than interacting with [BMIM][Ac]. The van der Waals force is weak and a long-distance force, thus ILs could be dried to some extent easily. It is consistent with Cuadradó-Prado's report which points out that water is adsorbed on the free surface of eight imidazolium based ionic liquids and could thus be easily removed.¹⁹ A slow absorption rate could also be witnessed for the hygroscopicity of many ILs in this stage.

Step 2 is a transition step with three substeps shown in Figure 2c–e. From 120 to 180 min (Step 2a), the bulk sorption also dominates the sorption (compared with Step 1), and only a slight surface sorption occurs. In general, Step 2a resembles Step 1. In Step 2a, there still exists some uninteracted acetate anions; the interaction is also strong although less anions participate than that in Step 1. On the other hand, water starts to interact with other water molecules by hydrogen-bonding networks, but showing a negligible extent until another turning point at 180 min, as shown in Figure 6. Thus, in this substep, alternation of OH_s , C_{2,4,5H}, C_{alkyl}H, and OH_b also exists but with a slower rate than that in Step 1 (Figure 7).

From 180 to 260 min (Step 2b), bulk sorption and surface sorption is comparative. In Step 2b, negligible anion is available to uptake atmospheric water by hydrogen bonding interaction. Thus, water mainly forms a hydrogen-bonding network with the absorbed water, which could be corroborated by the turning point of OH_b in Figure 6. Figure 7 also shows that from 180 to 260 min, the anion environment indicated by OH_b almost has no change rate in intensity. However, the change rate of C_{2,4,5H} still changes, implying still-existing CH–water interactions after 180 min despite the disappearance of water–anion interaction. In this part, C_{2,4,5H} interacts with water more directly and stronger than in Step 1 and Step 2a because of being free from the attachment of an anion, thus a smaller increase in blue shift and peak intensity occurs in this stage (Figure 1).

From 260 to 320 min (Step 2c), the surface sorption takes up the largest part of the sorption, while bulk sorption is small. In general, Step 2c resembles Step 3. In Step 2c, the groups (i.e., anion, C_{2H}, C_{4,5H}) that are able to interact with water have already interacted; the distance that is able to expand has already reached its limit under the conditions considered. The most possible place for atmospheric water to interact with [BMIM][Ac] is the surface of this IL. The change rate is thus very low and stable, as shown in Figures 6 and 7.

3.5. Quantifying the Surface vs Bulk Atmospheric Water Sorption in [BMIM][Ac]. The conclusion drawn from s-PCM2D-COS (Figure 6) suggests that 320 min is a turning point, after which water is absorbed only on the surface. The as-PCM2D-COS (Figure 7) gives another turning point at 120 min, before which water is absorbed only into the bulk. Considering the two turning points, the dynamic process of atmospheric water sorption by [BMIM][Ac] could be described as below. At the first 120 min, only bulk sorption occurs (Step 1). From 120 to 320 min, bulk sorption and surface sorption occurs simultaneously (Step 2). After 320 min, only surface sorption occurs (Step 3). Specifically, Step 2 consists of three substeps, Step 2a (120–180 min), Step 2b (180–260 min), and Step 2c (260–320 min), with the bulk sorption taking up the most part, about one-half, and small part of the total sorption, respectively.

On the basis of the clarification of the dynamic water sorption process, we then quantify the bulk versus surface water sorption in [BMIM][Ac] by combining with its atmospheric water sorption kinetic. The process of water absorbed in ILs could be well fitted by the modified-two-step model, i.e., $W = W_\infty(1 - \exp(-kt))$, where W , W_∞ , k , t represent sorption capacity (g H₂O/g ILs), steady-state sorption capacity (g H₂O/g ILs), model parameter (h⁻¹), and time (h), respectively.²⁴

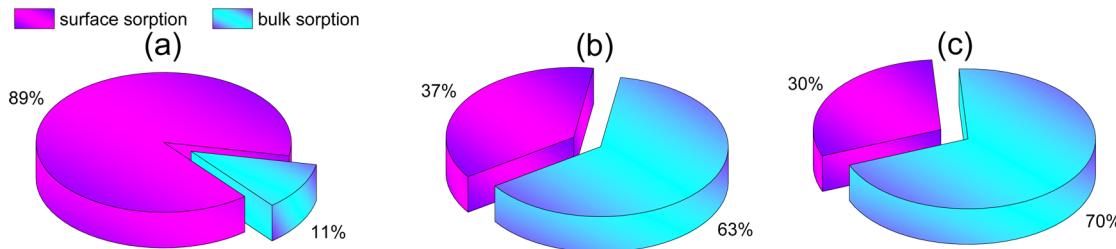


Figure 8. Proportion of atmospheric water absorbed into the bulk and surface of ILs [BMIM][Ac] until steady-state (a), within 360 min (b), and within 320 min (c).

This modified-two-step model is aimed to unify the first step with a fast linear ($W = k_1 t$, $t \leq t_0$) water absorption kinetic into the bulk ILs and the second step with a slow exponential ($W = W_\infty(1 - \exp(-k_2 t))$, $t \geq t_0$) adsorption kinetic on the surface of ILs by just one equation $W = W_\infty(1 - \exp(-kt))$.²⁰ The possible reason is that the dividing time point t_0 is hard to determine in practice; the value of $W_\infty(1 - \exp(-kt))$ is equivalent to kt when the time t is close to zero, which could be always approached due to the relatively short time period of linearly absorption.²⁰ This modified-two-step model has been well applied for the hygroscopicity of many kinds of ILs as a function of time.^{57–60} A more direct evidence for the modified-two-step model is from the proposed three-steps atmospheric water sorption in [BMIM][Ac] derived here by IR PCMW2D-COS. The difference is that the conclusion here gives a transition step (Step 2) compared to our previous proposed modified-two-step model. Namely, the transition points here derived by 2D-COS compensate for the shortcomings of neglecting the dividing time point t_0 of the previous modified-two-step model. Thus, this modified-two-step model is applicable to the water absorption in ILs, including [BMIM]-[Ac]. Specifically, here for [BMIM][Ac], the related parameters are listed as below: $W_\infty = 25.16\%$ g H₂O/g ILs; $k = 0.0319\text{ h}^{-1}$.²⁴ Therefore, the water sorption capacity at 0 min, 120 min, 320 min, 360 min, and steady-state ($t = \infty$) could be derived as 0 ($W_{0\text{ min}}$), 1.55% ($W_{120\text{ min}}$), 3.93% ($W_{320\text{ min}}$), 4.38% ($W_{360\text{ min}}$), and 25.16% (W_∞) g H₂O/g ILs, respectively.

The bulk sorption and surface sorption are comparative in Step 2 after considering the averaging effect of all the three substeps, thus, the capacity of the bulk and surface sorption until steady-state could be derived as 2.74% g H₂O/g ILs and 22.41% g H₂O/g ILs by eq 1 and 2, respectively. Then, by eqs 3 and 4, the proportion of bulk and surface water sorption until steady state could be calculated as 11% and 89%, respectively (Figure 8a). Note that the above conclusions derived from these equations (eqs 1–8) are based on the following assumption: before 120 min only bulk sorption of atmospheric water in [BMIM][Ac] occurs; after 320 min only surface sorption takes place; between 120 min and 320 min the bulk sorption and surface sorption are comparative, that is, the same; in the whole process the water sorption could be described by the modified-two-step model $W = W_\infty(1 - \exp(-kt))$. About 89% surface water sorption by [BMIM][Ac] until steady-state suggests that most of the atmospheric water would adsorbed on the surface of IL [BMIM][Ac], while the remaining water is absorbed into the [BMIM][Ac] bulk under a nearly equilibrating condition. However, a different conclusion for the hygroscopicity of eight imidazolium-based ILs drawn by Cuadrado-Prado indicated that all the water was adsorbed in the free surface of the ILs sample physically by forming a thin film on the ILs surface.¹⁹ This difference might be due to the

higher hydrophobicity of ILs (i.e., [C_nMIM][BF₄] and [EMIM][C_nOSO₃] with $n = 2, 4, 6, 8$) by Cuadrado-Prado than our IL sample (i.e., [BMIM][Ac]) due to the presence of higher hydrophilic acetate anion,^{19,20} thus some of atmospheric water could enter into the [BMIM][Ac] bulk part via strong hydrogen-bonding with the acetate anion.

Furthermore, within 360 min, the amount of water sorption in bulk [BMIM][Ac] could be calculated with eq 5, i.e., 2.74% g H₂O/g ILs. Note that in this case, the bulk sorption is equal to that of the steady-state. The amount of surface water sorption could be derived as 1.63% g H₂O/g IL by using eq 6. Thus, the proportion of bulk and surface water uptake from the moist air by [BMIM][Ac] within 360 min is about 63% and 37%, respectively (Figure 8b). Similarly, during the first 320 min, bulk proportion and surface proportion amounts to 70% and 30%, respectively, by using eqs 7 and 8 (Figure 8c). These results imply that exposing [BMIM][Ac] to the atmospheric water environment under a relative short-term would make some of the moisture enter the interior of [BMIM][Ac]. The possible reason is the presence of free acetate anion that draws the water molecules with high affinity.

$$W_{\text{bulk-steady}} = (W_{120\text{min}} - W_{0\text{min}}) + (W_{320\text{min}} - W_{120\text{min}})/2 \quad (1)$$

$$W_{\text{surface-steady}} = (W_{\infty\text{min}} - W_{320\text{min}}) + (W_{320\text{min}} - W_{120\text{min}})/2 \quad (2)$$

$$X_{\text{bulk-steady}} = W_{\text{bulk}}/(W_{\text{bulk}} + W_{\text{surface}}) \quad (3)$$

$$X_{\text{surface-steady}} = W_{\text{surface}}/(W_{\text{bulk}} + W_{\text{surface}}) \quad (4)$$

$$W_{\text{bulk-360min}} = (W_{120\text{min}} - W_{0\text{min}}) + (W_{320\text{min}} - W_{120\text{min}})/2 \quad (5)$$

$$W_{\text{surface-360min}} = (W_{360\text{min}} - W_{320\text{min}}) + (W_{320\text{min}} - W_{120\text{min}})/2 \quad (6)$$

$$W_{\text{bulk-320min}} = (W_{120\text{min}} - W_{0\text{min}}) + (W_{320\text{min}} - W_{120\text{min}})/2 \quad (7)$$

$$W_{\text{surface-320min}} = (W_{320\text{min}} - W_{300\text{min}}) + (W_{300\text{min}} - W_{120\text{min}})/2 \quad (8)$$

4. CONCLUSION

The dynamic process of the atmospheric water absorbed in [BMIM][Ac] could be described as three steps in sequence: only bulk sorption via hydrogen-bonding interaction at the first 120 min (Step 1); bulk sorption and surface sorption

simultaneously via both hydrogen-bonding interaction and van der Waals force from 120 to 320 min (Step 2); and only surface sorption via van der Waals force from 320 min to steady state (Step 3). Specifically, Step 2 consists of three substeps. In Step 2a, mainly bulk sorption takes place and only little surface sorption occurs (120–180 min). As time passes by, the ratio of surface sorption to bulk sorption increases. In Step 2b (180–260 min), surface sorption and bulk sorption is comparative, while in the consecutive Step 2c (260–320 min), the surface sorption is dominating.

More interestingly, the atmospheric water could be deemed as a probe for detecting the chemical structure of [BMIM][Ac] during Step 1. The results show that one anion is surrounded by three C₄SH molecules, and two anions are surrounded by five C₂H molecules via hydrogen bonds, which is very susceptible to water moisture especially for the former one. The remaining anions form multimers (i.e., pentamer, equilibrating with one dimer and one trimer) by hydrogen-bonding interaction, which is not affected by the absorption of atmospheric water. The alkyl tethered to the cation ring aggregates to some extent by van der Walls force, which is moderately susceptible to the water attack. The stack among rings of the cations is negligible.

Furthermore, the proportion of bulk atmospheric water sorption and surface sorption in [BMIM][Ac] is quantified as about 70% and 30% within 320 min, 63% 37% during the entire experimental time (360 min), and 11% and 89% from 320 min to steady state, respectively.

The underlying meaning is that pure [BMIM][Ac] is easily contaminated by the atmospheric water than the water-mixed ILs. The difficulty in drying ILs to maintain a very low content of water is due to the strong hydrogen-bonding interaction between water and anions (rather than van der Waals force). This finding also suggests that it would be better to avoid mixing or oscillating behavior for water and ILs, because the surface-atmospheric-water sorption in ILs via weak van der Waals force would transform to the bulk-atmospheric-water sorption in ILs via strong hydrogen-bonding interaction, hence making it more difficult to dry. Furthermore, for the application of ILs (e.g., AcIL including [BMIM][Ac]) in biomass dissolution or other usage (e.g., sour gases capture,⁶¹ catalyst, or solvent), the robust atmospheric water sorption in ILs would hinder the utilization of ILs enormously. For example, the robust atmospheric water (Step 1) absorbed in biomass-dissolved ILs might rob the ILs via strong hydrogen bonds from the biomass, while the surface water sorption might have a minor effect on the application, because the water would stay on the surface via a weak van der Walls force.

AUTHOR INFORMATION

Corresponding Author

*Tel.: +86-10-62514925. Fax: +86-10-62516444. E-mail: tcmu@chem.ruc.edu.cn.

Notes

The authors declare no competing financial interest.

ACKNOWLEDGMENTS

This work was supported by the National Natural Science Foundation of China (21173267). The authors also thank Morita and Ozaki for help on obtaining PCMW2D-COS with the software 2D shige.

REFERENCES

- Earle, M. J.; Seddon, K. R. Ionic Liquids. Green Solvents for the Future. *Pure Appl. Chem.* **2000**, *72*, 1391–1398.
- Wang, H.; Gurau, G.; Rogers, R. D. Ionic Liquid Processing of Cellulose. *Chem. Soc. Rev.* **2012**, *41*, 1519–1537.
- Kosan, B.; Michels, C.; Meister, F. Dissolution and Forming of Cellulose with Ionic Liquids. *Cellulose* **2008**, *15*, 59–66.
- Zhao, H.; Baker, G. A.; Song, Z.; Olubajo, O.; Crittle, T.; Peters, D. Designing Enzyme-Compatible Ionic Liquids That Can Dissolve Carbohydrates. *Green Chem.* **2008**, *10*, 696–705.
- Xie, H.; Zhang, S.; Li, S. Chitin and Chitosan Dissolved in Ionic Liquids as Reversible Sorbents of CO₂. *Green Chem.* **2006**, *8*, 630–633.
- Chen, Q.; Xu, A.; Li, Z.; Wang, J.; Zhang, S. Influence of Anionic Structure on the Dissolution of Chitosan in 1-Butyl-3-Methylimidazolium-Based Ionic Liquids. *Green Chem.* **2011**, *13*, 3446–3452.
- Wu, Y.; Sasaki, T.; Irie, S.; Sakurai, K. A Novel Biomass-Ionic Liquid Platform for the Utilization of Native Chitin. *Polymer* **2008**, *49*, 2321–2327.
- Ding, Z.-D.; Chi, Z.; Gu, W.-X.; Gu, S.-M.; Liu, J.-H.; Wang, H.-J. Theoretical and Experimental Investigation on Dissolution and Regeneration of Cellulose in Ionic Liquid. *Carbohyd. Polym.* **2012**, *89*, 7–16.
- Jaworska, M. M.; Kozlecki, T.; Gorak, A. Review of the Application of Ionic Liquids as Solvents for Chitin. *J. Polym. Eng.* **2012**, *32*, 67–69.
- Zhuo, K. L.; Chen, Y. J.; Chen, J.; Bai, G. Y.; Wang, J. J. Interactions of 1-Butyl-3-Methylimidazolium Carboxylate Ionic Liquids with Glucose in Water: A Study of Volumetric Properties, Viscosity, Conductivity, and NMR. *Phys. Chem. Chem. Phys.* **2011**, *13*, 14542–14549.
- Zhao, Y.; Liu, X.; Wang, J.; Zhang, S. Insight into the Cosolvent Effect of Cellulose Dissolution in Imidazolium-Based Ionic Liquid Systems. *J. Phys. Chem. B* **2013**, *117*, 9042–9049.
- Liu, W. N.; Hou, Y. C.; Wu, W. Z.; Ren, S. H.; Jing, Y.; Zhang, B. G. Solubility of Glucose in Ionic Liquid + Antisolvent Mixtures. *Ind. Eng. Chem. Res.* **2011**, *50*, 6952–6956.
- Youngs, T. G.; Holbrey, J. D.; Mullan, C. L.; Norman, S. E.; Lagunas, M. C.; D'Agostino, C.; Mantle, M. D.; Gladden, L. F.; Bowron, D. T.; Hardacre, C. Neutron Diffraction, NMR and Molecular Dynamics Study of Glucose Dissolved in the Ionic Liquid 1-Ethyl-3-Methylimidazolium Acetate. *Chem. Sci.* **2011**, *2*, 1594–1605.
- Fendt, S.; Padmanabhan, S.; Blanch, H. W.; Prausnitz, J. M. Viscosities of Acetate or Chloride-Based Ionic Liquids and Some of Their Mixtures with Water or Other Common Solvents. *J. Chem. Eng. Data* **2010**, *56*, 31–34.
- Römic, C.; Merkel, N. C.; Valbonesi, A.; Schaber, K.; Sauer, S.; Schubert, T. J. S. Thermodynamic Properties of Binary Mixtures of Water and Room-Temperature Ionic Liquids: Vapor Pressures, Heat Capacities, Densities, and Viscosities of Water + 1-Ethyl-3-Methylimidazolium Acetate and Water + Diethylmethylammonium Methane Sulfonate. *J. Chem. Eng. Data* **2012**, *57*, 2258–2264.
- Quijada-Maldonado, E.; van der Boogaart, S.; Lijbers, J.; Meindersma, G.; de Haan, A. Experimental Densities, Dynamic Viscosities and Surface Tensions of the Ionic Liquids Series 1-Ethyl-3-Methylimidazolium Acetate and Dicyanamide and Their Binary and Ternary Mixtures with Water and Ethanol at T = (298.15 to 343.15 K). *J. Chem. Thermodyn.* **2012**, *51*, 51–58.
- Torrecilla, J. S.; Rafione, T.; Garcia, J.; Rodriguez, F. Effect of Relative Humidity of Air on Density, Apparent Molar Volume, Viscosity, Surface Tension, and Water Content of 1-Ethyl-3-Methylimidazolium Ethylsulfate Ionic Liquid. *J. Chem. Eng. Data* **2008**, *53*, 923–928.
- Tran, C. D.; Lacerda, S. H. D.; Oliveira, D. Absorption of Water by Room-Temperature Ionic Liquids: Effect of Anions on Concentration and State of Water. *Appl. Spectrosc.* **2003**, *57*, 152–157.
- Cuadrado-Prado, S.; Dominguez-Perez, M.; Rilo, E.; Garcia-Garabal, S.; Segade, L.; Franjo, C.; Cabeza, O. Experimental

- Measurement of the Hygroscopic Grade on Eight Imidazolium Based Ionic Liquids. *Fluid Phase Equilib.* **2009**, *278*, 36–40.
- (20) Cao, Y.; Chen, Y.; Sun, X.; Zhang, Z.; Mu, T. Water Sorption in Ionic Liquids: Kinetics, Mechanisms and Hydrophilicity. *Phys. Chem. Chem. Phys.* **2012**, *14*, 12252–12262.
- (21) Seddon, K. R.; Stark, A.; Torres, M. J. Influence of Chloride, Water, and Organic Solvents on the Physical Properties of Ionic Liquids. *Pure Appl. Chem.* **2000**, *72*, 2275–2287.
- (22) Cammarata, L.; Kazarian, S.; Salter, P.; Welton, T. Molecular States of Water in Room Temperature Ionic Liquids. *Phys. Chem. Chem. Phys.* **2001**, *3*, 5192–5200.
- (23) Cao, Y.; Sun, X.; Chen, Y.; Mu, T. Water Sorption in Amino-Acid Ionic Liquids: Kinetic, Mechanism, and Correlations between Hygroscopicity and Solvatochromic Parameters. *ACS Sustain. Chem. Eng.* **2013**, *2*, 138–148.
- (24) Chen, Y.; Cao, Y.; Mu, T. A New Application of Acetate-Based Ionic Liquids: Potential Usage as Drying Materials. *Chem. Eng. Technol.* **2014**, *37*, 1–9.
- (25) Hall, C. A.; Le, K. A.; Rudaz, C.; Radhi, A.; Lovell, C. S.; Damion, R. A.; Budtova, T.; Ries, M. E. Macroscopic and Microscopic Study of 1-Ethyl-3-methyl-imidazolium Acetate–Water Mixtures. *J. Phys. Chem. B* **2012**, *116*, 12810–12818.
- (26) Ding, Z. D.; Chi, Z.; Gu, W. X.; Gu, S. M.; Wang, H. J. Theoretical and Experimental Investigation of the Interactions between [Emim]Ac and Water Molecules. *J. Mol. Struct.* **2012**, *1015*, 147–155.
- (27) Brehm, M.; Weber, H.; Pensado, A. S.; Stark, A.; Kirchner, B. Proton Transfer and Polarity Changes in Ionic Liquid–Water Mixtures: A Perspective on Hydrogen Bonds from *ab Initio* Molecular Dynamics at the Example of 1-Ethyl-3-methylimidazolium Acetate–Water Mixtures—Part 1. *Phys. Chem. Chem. Phys.* **2012**, *14*, 5030–5044.
- (28) Shi, W.; Nulwala, H.; Achary, D. K.; Luebke, D. R. Theoretical and Experimental Studies of Water Interaction in Acetate Based Ionic Liquids. *Phys. Chem. Chem. Phys.* **2012**, *14*, 15897–15908.
- (29) Restolho, J.; Mata, J. L.; Colaço, R.; Saramago, B. J. Moisture Absorption in Ionic Liquid Films. *J. Phys. Chem. C* **2013**, *117*, 10454–10463.
- (30) Chen, Y.; Cao, Y.; Zhang, Y.; Mu, T. Hydrogen Bonding between Acetate-Based Ionic Liquids and Water: Three Types of IR Absorption Peaks and NMR Chemical Shifts Change Upon Dilution. *J. Mol. Struct.* **2014**, *1058*, 244–251.
- (31) Jiang, J.-C.; Lin, K.-H.; Li, S.-C.; Shih, P.-M.; Hung, K.-C.; Lin, S. H.; Chang, H.-C. Association Structures of Ionic Liquid/DMSO Mixtures Studied by High-Pressure Infrared Spectroscopy. *J. Chem. Phys.* **2011**, *134* (044506), 1–8.
- (32) Zhang, Q.; Wang, N.; Wang, S.; Yu, Z. Hydrogen Bonding Behaviors of Binary Systems Containing the Ionic Liquid 1-Butyl-3-methylimidazolium Trifluoroacetate and Water/Methanol. *J. Phys. Chem. B* **2011**, *115*, 11127–11136.
- (33) Wang, Y.; Li, H. R.; Han, S. J. A Theoretical Investigation of the Interactions between Water Molecules and Ionic Liquids. *J. Phys. Chem. B* **2006**, *110*, 24646–24651.
- (34) Gao, Y.; Zhang, L.; Wang, Y.; Li, H. Probing Electron Density of H-Bonding between Cation–Anion of Imidazolium-Based Ionic Liquids with Different Anions by Vibrational Spectroscopy. *J. Phys. Chem. B* **2010**, *114*, 2828–2833.
- (35) Zhang, L.; Xu, Z.; Wang, Y.; Li, H. Prediction of the Solvation and Structural Properties of Ionic Liquids in Water by Two-Dimensional Correlation Spectroscopy. *J. Phys. Chem. B* **2008**, *112*, 6411–6419.
- (36) Zhang, Q.; Wang, N.; Yu, Z. The Hydrogen Bonding Interactions between the Ionic Liquid 1-Ethyl-3-methylimidazolium Ethyl Sulfate and Water. *J. Phys. Chem. B* **2010**, *114*, 4747–4754.
- (37) Wang, N.; Zhang, Q.; Wu, F.; Li, Q.; Yu, Z. Hydrogen Bonding Interactions between a Representative Pyridinium-Based Ionic Liquid [BuPy][BF₄] and Water/Dimethyl Sulfoxide. *J. Phys. Chem. B* **2010**, *114*, 8689–8700.
- (38) Sun, B.; Wu, P. Trace of the Thermally Induced Evolution Mechanism of Interactions between Water and Ionic Liquids. *J. Phys. Chem. B* **2010**, *114*, 9209–9219.
- (39) Sun, B.; Jin, Q.; Tan, L.; Wu, P.; Yan, F. Trace of the Interesting “V”-Shaped Dynamic Mechanism of Interactions between Water and Ionic Liquids. *J. Phys. Chem. B* **2008**, *112*, 14251–14259.
- (40) López-Pastor, M.; Ayora-Cañada, M. J.; Valcárcel, M.; Lendl, B. Association of Methanol and Water in Ionic Liquids Elucidated by Infrared Spectroscopy Using Two-Dimensional Correlation and Multivariate Curve Resolution. *J. Phys. Chem. B* **2006**, *110*, 10896–10902.
- (41) Wu, B.; Zhang, Y.; Wang, H. Insight into the Intermolecular Interactions in [Bmim]BF₄/[Amim]Cl–Ethanol–Water Mixtures by Near-Infrared Spectroscopy. *J. Phys. Chem. B* **2009**, *113*, 12332–12336.
- (42) He, H.; Chen, H.; Zheng, Y.; Zhang, X.; Yao, X.; Yu, Z.; Zhang, S. The Hydrogen-Bonding Interactions between 1-Ethyl-3-Methylimidazolium Lactate Ionic Liquid and Methanol. *Aust. J. Chem.* **2012**, *66*, 50–59.
- (43) Takamuku, T.; Kyoshin, Y.; Shimomura, T.; Kittaka, S.; Yamaguchi, T. Effect of Water on Structure of Hydrophilic Imidazolium-Based Ionic Liquid. *J. Phys. Chem. B* **2009**, *113*, 10817–10824.
- (44) Mele, A.; Tran, C. D.; De Paoli Lacerda, S. H. The Structure of a Room-Temperature Ionic Liquid with and without Trace Amounts of Water: The Role of C-H···O and C-H···F Interactions in 1-N-Butyl-3-methylimidazolium Tetrafluoroborate. *Angew. Chem., Int. Ed.* **2003**, *115*, 4500–4502.
- (45) Takamuku, T.; Honda, Y.; Fujii, K.; Kittaka, S. Aggregation of Imidazolium Ionic Liquids in Molecular Liquids Studied by Small-Angle Neutron Scattering and NMR. *Anal. Sci.* **2008**, *24*, 1285–1290.
- (46) Shimomura, T.; Takamuku, T.; Yamaguchi, T. Clusters of Imidazolium-Based Ionic Liquid in Benzene Solutions. *J. Phys. Chem. B* **2011**, *115*, 8518–8527.
- (47) Ficke, L. E.; Brennecke, J. F. Interactions of Ionic Liquids and Water. *J. Phys. Chem. B* **2010**, *114*, 10496–10501.
- (48) Li, W.; Zhang, Z.; Han, B.; Hu, S.; Xie, Y.; Yang, G. Effect of Water and Organic Solvents on the Ionic Dissociation of Ionic Liquids. *J. Phys. Chem. B* **2007**, *111*, 6452–6456.
- (49) Miki, K.; Westh, P.; Nishikawa, K.; Koga, Y. Effect of an “Ionic Liquid” Cation, 1-Butyl-3-methylimidazolium, on the Molecular Organization of H₂O. *J. Phys. Chem. B* **2005**, *109*, 9014–9019.
- (50) Katayanagi, H.; Nishikawa, K.; Shimozaki, H.; Miki, K.; Westh, P.; Koga, Y. Mixing Schemes in Ionic Liquid–H₂O Systems: A Thermodynamic Study. *J. Phys. Chem. B* **2004**, *108*, 19451–19457.
- (51) Noda, I. Two-Dimensional Infrared Spectroscopy. *J. Am. Chem. Soc.* **1989**, *111*, 8116–8118.
- (52) Noda, I. Two-Dimensional Infrared (2D IR) Spectroscopy: Theory and Applications. *Appl. Spectrosc.* **1990**, *44*, 550–561.
- (53) Thomas, M.; Richardson, H. H. Two-Dimensional FT-IR Correlation Analysis of the Phase Transitions in a Liquid Crystal, 4'-N-Octyl-4-cyanobiphenyl (8CB). *Vib. Spectrosc.* **2000**, *24*, 137–146.
- (54) Morita, S.; Shinzawa, H.; Noda, I.; Ozaki, Y. Perturbation-Correlation Moving-Window Two-Dimensional Correlation Spectroscopy. *Appl. Spectrosc.* **2006**, *60*, 398–406.
- (55) Russina, O.; Fazio, B.; Di Marco, G.; Caminiti, R.; Triolo, A., Structural Organization in Neat Ionic Liquids and in Their Mixtures. In *The Structure of Ionic Liquids, Soft and Biological Matter*; Springer: New York, 2014; pp 39–61.
- (56) Bowron, D.; D'Agostino, C.; Gladden, L.; Hardacre, C.; Holbrey, J.; Lagunas, M.; McGregor, J.; Mantle, M.; Mullan, C.; Youngs, T. Structure and Dynamics of 1-Ethyl-3-Methylimidazolium Acetate via Molecular Dynamics and Neutron Diffraction. *J. Phys. Chem. B* **2010**, *114*, 7760–7768.
- (57) Di Francesco, F.; Calisi, N.; Creatini, M.; Melai, B.; Salvo, P.; Chiappe, C. Water Sorption by Anhydrous Ionic Liquids. *Green Chem.* **2011**, *13*, 1712–1717.

- (58) Cao, Y.; Chen, Y.; Lu, L.; Xue, Z.; Mu, T. Water Sorption in Functionalized Ionic Liquids: Kinetics and Intermolecular Interactions. *Ind. Eng. Chem. Res.* **2013**, *52*, 2073–2083.
- (59) Chen, Y.; Cao, Y.; Lu, X.; Zhao, C.; Yan, C.; Mu, T. Water Sorption in Protic Ionic Liquids: Correlation between Hygroscopicity and Polarity. *New J. Chem.* **2013**, *37*, 1959–1967.
- (60) Arellano, I. H. J.; Guarino, J. G.; Paredes, F. U.; Arco, S. D. Thermal Stability and Moisture Uptake of 1-Alkyl-3-methylimidazolium Bromide. *J. Therm. Anal. Calorim.* **2011**, *103*, 725–730.
- (61) Stevanovic, S.; Podgoršek, A.; Pádua, A. A. H.; Costa Gomes, M. F. Effect of Water on the Carbon Dioxide Absorption by 1-Alkyl-3-Methylimidazolium Acetate Ionic Liquids. *J. Phys. Chem. B* **2012**, *116*, 14416–14425.